analytical chemistry

pubs.acs.org/ac Article

Electron Acceptors Co-Regulated Self-Powered Photoelectrochemical Strategy and Its Application for Circulating Tumor Nucleic Acid Detection Coupled with Recombinase Polymerase Amplification

Xu Hun* and Yuchan Meng

Cite This: https://dx.doi.org/10.1021/acs.analchem.0c01893 Read Online

ACCESS | Metrics & More | Article Recommendations | Supporting Information

ABSTRACT: Biosensor working in a self-powered mode has been widely concerned because it produces a signal when the bias potential is 0 V. However, the self-powered mode is used only when the materials have self-powered properties. Conversion of non-self-powered to self-powered through molecular regulation can solve this problem effectively. Here, we fabricated a self-powered photoelectrochemical mode based on co-regulation of electron acceptors methylene blue (MB) and *p*-nitrophenol (*p*-NP). AuNPs@ZnSe nanosheet-modified gold electrode (AuNPs@ZnSeNSs/GE) gave a small photocurrent at 0 V. In the presence of MB and *p*-NP, AuNPs@ZnSeNSs/GE gave the strongest photocurrent at 0 V. Accordingly, an electron acceptor co-regulated self-powered photoelectrochemical assay was fabricated. As proof-of-concept demonstrations, this assay was applied for prostate cancer circulating tumor nucleic acid biomarker, *KLK2* and *PCA3*, detection combined with in situ recombinase polymerase amplification strategy. This assay generated a strong photocurrent and was sensitive to the variation of *KLK2* and *PCA3* concentration. The limits of detection were 30 and 32 aM, respectively. We anticipate this electron acceptor co-regulated self-powered photoelectrochemical mode to pave a new way for the development of self-powered sensing.

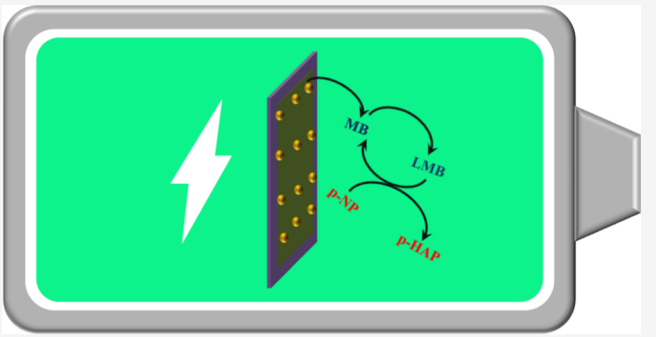

INTRODUCTION

Photoelectrochemical (PEC) analysis, as a burgeoning analytical method, has melded the advantages of both optical and electrochemical strategies such as easy operation, high sensitivity, simple design, and low cost.[1−5] PEC detection has attracted great attention.[6] However, nonspecific oxidations or reductions of redox-active interferences occurred when the high voltage is applied to the electrode.[7] Therefore, it is essential that PEC detection operates at a bias potential of 0 V. Self-powered PEC is put forward.[8] The self-powered PEC sensor permits detection at 0 V bias potential, averting the common necessity of the high bias potential.[9−11] At the same time, because there is no high bias potential in the detection process, the interference of pollutants was eliminated.[12]

In recent studies, self-powered PEC sensors are almost built based on the photoelectric performance of the material itself, that is, the self-powered PEC sensor is built when the material has a good response at 0 V bias potential. Several related studies are focused on the enhancement of self-powered PEC performance by materials strategies achieved by compounding multiple-functional nanomaterials.[13] For example, Han et al. developed a self-powered PEC biosensor based on a Au@BiOI/NiO heterostructure.[14] Tian et al., combined an n-type cobalt phosphide double-shelled hollow nanocage with p-type Cu_2O to develop a self-powered photoelectrogenic cathode and applied it for glucose detection.[15] Çakıroğlu et al. modified supercapacitor carbon nanotubes and Co_3O_4 onto the anatase TiO_2-coated indium tin oxide electrodes to construct a self-powered PEC biosensor for detection of glucose.[16] Gurudayal et al. established a Si photocathode with a Ag-supported dendritic Cu catalyst, which was used in self-powered CO_2 reduction device.[17] In these self-powered PEC sensors, few kinds of electron acceptors or donors such as O_2 or H_2O_2 are usually used to enhance the PEC response.[18,19] In another case, PEC signals can be enhanced by the targets, such as gallic acid[8] and glutathione.[13] And steric hindrance is also used for changing PEC signal without electron acceptors or donors.[20,21]

From the existing research reports, it is found that the design and synthesis of photoactive materials for the fabrication of

Received: May 3, 2020
Accepted: August 3, 2020

self-powered PEC detection is crucial. There are no works based on adjusting the kinds of electron donors or acceptors for the fabrication of self-powered PEC sensing. Hence, an idea was put forward that whether there was a phenomenon of conversion from non-self-powered PEC to self-powered PEC under certain circumstances. It was positive. During our experiment, it was found that a nanocomposite, AuNPs@ZnSeNSs, modified gold electrode (AuNPs@ZnSeNSs/GE) with the optimal PEC response at −0.2 V potential. Nevertheless, when the PEC response of AuNPs@ZnSeNSs/GE was exhibited in the mixture of methylene blue (MB) and *p*-nitrophenol (*p*-NP), the optimal PEC response potential was changed to 0 V potential. This exciting discovery suggested that the non-self-powered PEC can be changed to self-powered PEC by adjusting the kinds of electron acceptors instead of making new substances. The electron acceptors, MB and *p*-NP, co-regulated self-powered PEC response of AuNPs@ZnSeNSs/GE was studied systemically. A PEC assay based on electron acceptors co-regulated self-powered PEC coupled with in situ recombinase polymerase amplification (RPA) and in situ generating *p*-NP by alkaline phosphatase catalyzing *p*-nitrophenyl phosphate disodium salt hexahydrate (*p*-NPP) was developed.

EXPERIMENTAL SECTION

Synthesis of AuNPs@ZnSeNSs. The bulk ZnSe was exfoliated via an ultrasonic exfoliation method to obtain ZnSe nanosheets (ZnSeNSs). Details of the preparation of ZnSeNSs are described in the Supporting Information, (S2). AuNPs@ZnSeNSs were fabricated through in situ growth.[22] ZnSeNSs (3 mL, 5 mg/mL) and $HAuCl_4{\cdot}4H_2O$ (1 mL, 10 mg/mL) were added into a flask, which was heated to 115 °C by an oil bath under stirring. The solution was continued to reflux and stirred for 3 min to ensure that the $AuCl_4^-$ ions adsorb onto ZnSeNSs. Then, 1 mL (equal volume to $HAuCl_4{\cdot}4H_2O$) of 6.66 mg/mL sodium citrate solution was dropped into the flask. The mixture was refluxed at 115 °C for 3 min to obtain the black AuNPs@ZnSeNSs. The final black precipitate was collected by centrifugation (14 000 rpm, 10 min). Different masses of tetrachloroauric acid can affect the PEC signal. The mass ratios of ZnSeNSs to $HAuCl_4{\cdot}4H_2O$ of 1:0.2, 1:0.33, 1:0.66, 1:1, and 1:1.5 were studied (S3). The effect of reaction time and heating temperature on the PEC signal was also studied (S4).

Electrochemical and Photoelectrochemical Measurements. Cyclic voltammogram (CV) was measured in a 0.1 M phosphate buffer (pH 7.4) using a gold electrode as the working electrode, a Pt wire as the counter electrode, and a Ag/Ag^+ as the reference electrode. The modified electrode was inserted into a phosphate buffer, which was deoxidized with nitrogen for 30 min, and cyclic voltammetry was performed under an inert atmosphere with potential ranging from −2.0 to 2.0 V and a scan rate of 0.1 V s^{-1}.

To investigate the mechanism of MB and *p*-NP co-regulated self-powered PEC strategy, the CV of AuNPs@ZnSeNSs/GE was measured in a 0.1 mM MB solution, a 1.0 mM *p*-NP solution, or a mixture of MB and *p*-NP solutions (0.1 mM MB, 1.0 mM *p*-NP), respectively, with potential ranging from −1.1 to 0.2 V and a scan rate of 0.1 V s^{-1}. The electrochemical impedance spectroscopy (EIS) response of the electrode stepwise modification process was measured in 5.0 mM $[Fe(CN)_6]^{3-/4-}$ containing 0.1 M KCl. The PEC signal was measured in pH 7.4 0.1 M phosphate buffer containing 1 mM *p*-NPP and 0.1 M MB irradiated with a 10 W LED lamp. The light was switched off, on, and off for 10 s each under 0 V potential.

***KLK2* and *PCA3* Detection.** First, 15 μL of AuNPs@ZnSeNSs was dropped onto the surface of the gold electrode and dried naturally in air. Then, 10 μL of 10 mM TCEP was added into 40 μL of 10 μM thiolated forward primer (SH-FP), and the mixture was incubated at 37 °C with shaking. After 60 min, 10 μL of the mixture was added onto the surface of AuNPs@ZnSeNSs/GE and incubated for 2 h at 37 °C to get FP/AuNPs@ZnSeNSs/GE. Then, FP/AuNPs@ZnSeNSs/GE was immersed in a 1 mM MCH solution for 0.5 h. Next, the RPA solution was prepared for the surface amplification of the *KLK2* gene. The RPA reaction solution was made of 2.4 μL of biotin-reverse primer (biotin-RP) (10 μM), 13.2 μL of DNase-free water, 29.5 μL of rehydration buffer, and 2.5 μL of magnesium acetate (280 mM).[23] Then, 10 μL of the above reaction mixture and 5 μL of the *KLK2* sample were added onto the surface of FP/AuNPs@ZnSeNSs/GE. After amplification for 30 min at 37 °C, the electrode was washed with 0.1 M phosphate buffer. Finally, the electrodes were incubated with 10 μL of 1 μM SA-ALP for 30 min at 37 °C and washed with 0.1 M phosphate buffer before PEC measurement. *PCA3* detection steps are the same as *KLK2*.

RESULTS AND DISCUSSION

Morphology and Elemental Analysis Characterization of ZnSeNSs and AuNPs@ZnSeNSs. The transmission electron microscopy (TEM) images of exfoliated ZnSe and bulk ZnSe are shown in Figure 1A,B. It was clearly seen that

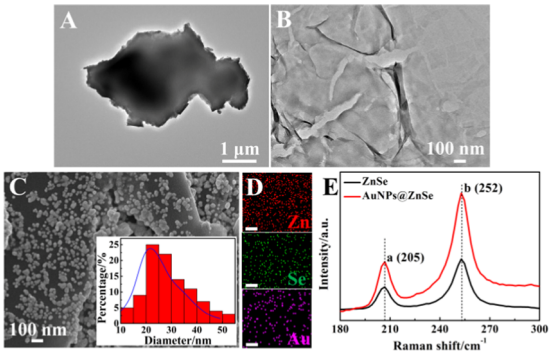

Figure 1. TEM images of bulk ZnSe (A) and ZnSeNSs (B). SEM image of AuNPs@ZnSeNSs and size distribution of AuNPs (inset) (C). Elemental mapping image of AuNPs@ZnSeNSs (D). Raman spectrum of ZnSe and AuNPs@ZnSeNSs (E).

bulk ZnSe was an irregular bulk structure with a very thick layer (Figure 1A), while after exfoliation, ZnSeNSs showed a thin sheetlike structure (Figure 1B). It demonstrated convincingly that the layers of ZnSeNSs were fewer than those of pristine ZnSe. The TEM images of ZnSeNSs and bulk ZnSe proved that the ultrasonic exfoliation method was practical and effective.

After deposition of AuNPs, as shown in Figure 1C, the surface of AuNPs@ZnSeNSs became rough, which proved that AuNPs@ZnSeNSs had loaded a large number of AuNPs. AuNPs were distributed homogeneously on the surface of ZnSeNSs. AuNPs were approximately spherical with size of about 26 ± 3 nm (inset in Figure 1C). Then, the elemental distributions of Zn, Se, and Au of AuNPs@ZnSeNSs were

https://dx.doi.org/10.1021/acs.analchem.0c01893
Anal. Chem. XXXX, XXX, XXX−XXX

characterized using elemental mapping (Figure 1D). Zn, Se, and Au elements are homogeneous and continuously distributed. This phenomenon indicated that AuNPs were loaded onto ZnSeNSs successfully. Figure 1E shows the Raman spectra of ZnSeNSs and AuNPs@ZnSeNSs. The Raman spectrum was recorded, and the wavelength of the scattering light was 532 nm. In the Raman spectrum of ZnSeNSs, two major peaks located at 205 and 252 cm^{-1} can be observed. The Raman peaks at 205 and 252 cm^{-1} correspond to the transverse optic (TO) phonon modes and longitudinal optic (LO) phonon modes of ZnSeNSs.[24] From Figure 1E, it was shown that the Raman signals of AuNPs@ZnSeNSs were all enhanced compared to that of ZnSeNSs. That was caused by the surface-enhanced Raman spectroscopy (SERS) activity that is related to coupling of the SPR of adjacent AuNPs.[25] And the SERS leads to the generation of plasmonic "hot spots", which has shown extremely high enhancement in the Raman response of the coupled AuNPs.[26] These results indicated that AuNPs@ZnSeNSs were synthesized successfully.

Establishment of Electron Acceptors Co-Regulated Self-Powered PEC. After Willner and Katz coined the term "self-powered biosensor" for a biofuel cell in 2001,[27] the concept of self-power was used in various fields, such as electrochemistry,[28] biofuel cell,[29] phototelechemistry,[15] photodetectors,[30] human tissue engineering scaffold,[31] social robotics,[11,32] etc. Self-powered biosensor is defined as a biosensor operated without external voltage or operated at 0 V. In 2015, Zhang et al. reported pioneered self-powered PEC biosensing.[33,34] This self-powered biosensor has no need of voltage bias. Such a unique feature makes redox-active interferences free from the nonspecific oxidation or reduction upon the application of the potential on the electrode. It was promising for batteryless, miniature size biosensing devices.[35] In this work, a novel self-powered PEC tactic was reported. AuNPs@ZnSeNSs/GE gave the strongest PEC response at −0.2 V potential in phosphate buffer. Nevertheless, in the mixture of MB and *p*-NP, the strongest PEC response was changed to 0 V potential. This interesting finding was studied comprehensively. We called it co-regulated self-powered PEC strategy.

First, the PEC response of the AuNPs@ZnSeNS-modified GE was tested. The PEC response of AuNPs@ZnSeNSs/GE in phosphate buffer is shown in Figure 2A. The photocurrent was negative when the bias potential was 0 V. It indicates that the AuNPs@ZnSeNS-modified GE results in a cathode photocurrent. From −0.2 to 0.2 V, the photocurrent first decreased and then increased, and at 0 V, the photocurrent was so weak (curve c, −536 nA) that it cannot be used to construct a self-powered PEC strategy. In 0.1 mM MB, PEC response changed evidently. The intensity of PEC response increased (Figure 2B). The photocurrent first increased and then decreased from −0.2 to 0.2 V. At 0 V, the PEC response reached the maximum value of about −2857 nA (curve c). The enhancement of PEC response is ascribed to the reduction of MB by the photogenerated electron of AuNPs@ZnSeNSs. Beyond that, the direction of photocurrent was also deflected at 0.1 and 0.2 V. It suggests that MB not only amplifies the PEC response but also regulates the direction of the photocurrent. At the same time, the PEC intensity was also enhanced in 1.0 mM *p*-NP (Figure 2C) compared to that in phosphate buffer. But at 0 V, the PEC signal was still the lowest (curve c). When both MB and *p*-NP were present, the PEC response increased greatly under the measured bias potential (Figure 2D). The

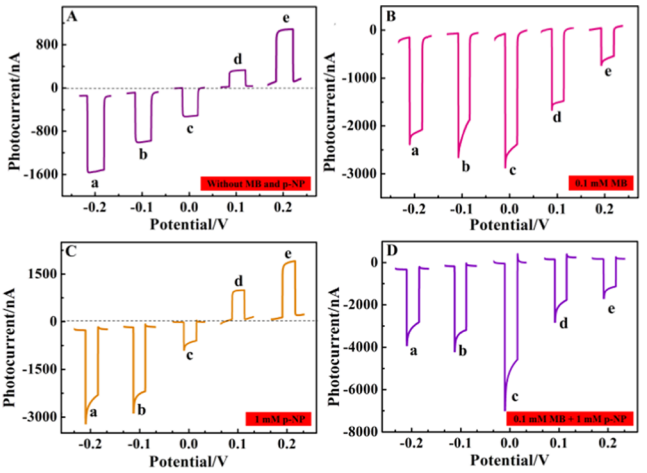

Figure 2. MB and *p*-NP co-regulated self-powered PEC response. AuNPs@ZnSeNS-modified GE in phosphate buffer without MB and *p*-NP (A) and containing 0.1 mM MB (B), 1 mM *p*-NP (C), and 0.1 mM MB and 1 mM *p*-NP (D).

photocurrent reached the maximum at 0 V, which suggests that *p*-NP can further amplify the signal and regulate optimal potential. Accordingly, the highest PEC response with the bias potential of 0 V can offer a new MB and *p*-NP co-regulated self-powered PEC sensing approach. Next, this co-regulated self-powered PEC was studied systematically.

At 0 V bias potential, the PEC response of AuNPs@ZnSeNS-modified GE in different solutions was evaluated, as depicted in Figure 3A. In the absence of MB and *p*-NP,

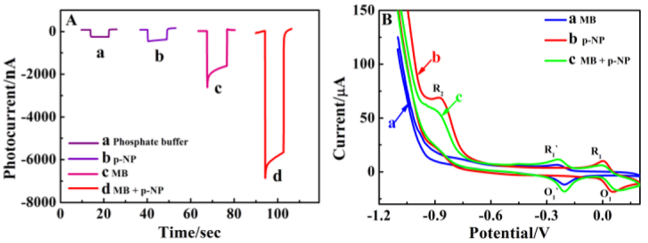

Figure 3. (A) PEC response of AuNPs@ZnSeNS-modified GE in phosphate buffer (0.1 M, pH 7.4) without MB and *p*-NP (curve a) and containing 1 mM *p*-NP (curve b), 0.1 mM MB (curve c), and 0.1 mM MB and 1 mM *p*-NP (curve d). (B) CV curves of AuNPs@ZnSeNS-modified GE in 0.1 M phosphate buffer (pH 7.4) containing 0.1 mM MB (curve a), 1 mM *p*-NP (curve b), and 0.1 mM MB and 1 mM *p*-NP (curve c). Scan rate: 200 mV/s.

AuNPs@ZnSeNS-modified GE had a low photocurrent (curve a), which was caused by the fast electron−hole recombination in AuNPs@ZnSeNSs. In addition, *p*-NP had a little effect on increasing the photocurrent (curve b), whereas MB can obviously enhance the photocurrent (curve c), which was ascribed to the electron transfer between MB and AuNPs@ZnSeNSs. MB as an electron acceptor can accept photogenerated electrons from the AuNPs@ZnSeNS photoelectrode. When the PEC response of the AuNPs@ZnSeNS-modified GE was tested in a 0.1 mM MB and 1 mM *p*-NP solution, a much higher signal was observed. It was caused by the regeneration of MB from the reaction between *p*-NP and leuco-methylene blue (LMB) (curve d). These results clearly demonstrate that the MB and *p*-NP co-regulated self-powered

https://dx.doi.org/10.1021/acs.analchem.0c01893
Anal. Chem. XXXX, XXX, XXX−XXX

PEC strategy has higher photocurrent at 0 V than the MB or *p*-NP separately regulated self-powered PEC strategy.

To investigate the mechanism of MB and *p*-NP co-regulated self-powered PEC strategy, the CV behaviors of AuNPs@ZnSeNS-modified GE were measured (Figure 3B). Curve a shows the CV of AuNPs@ZnSeNS-modified GE in an MB solution. It can be seen that there was a pair of redox peaks (R_1', O_1') between −0.25 and −0.20 V, which was ascribed to the transformation between MB and LMB.[36] As shown in curve b, AuNPs@ZnSeNS-modified GE in *p*-NP solution displayed three peaks (R_2, R_1, O_1). The irreversible peak R_2 at −0.858 V was attributed to the direct reduction of *p*-NP into phydroxylaminophenol (*p*-HAP), and a pair of redox peaks at 0−0.06 V was attributed to the transformation between p-HAP and p-nitrosophenol (*p*-NSP).[37,38] As shown in curve c, in the MB and *p*-NP solution, AuNPs@ZnSeNS-modified GE exhibited lower reductive peaks of *p*-NP (R_2, R_1, O_1). That is because the *p*-NP participates in the oxidation of LMB and leads to the consumption of *p*-NP (S6, Figure S4). Since *p*-NP participates in the redox of MB, the redox peak of MB (R_1', O_1') was enhanced. Combined with the above experimental results, MB gave relatively large PEC response, *p*-NP gave relatively small PEC response, but the mixture of MB and *p*-NP greatly enhanced the PEC intensity, from which it is concluded that *p*-NP can accelerate the regeneration of MB. Therefore, in the presence of MB and *p*-NP, the PEC response and the redox peak of MB are all enlarged.

The mass ratio of ZnSeNSs to $HAuCl_4{\cdot}4H_2O$ was also investigated for it affecting the PEC response greatly. The maximum photocurrent responses occurred at the mass ratio of ZnSeNSs to $HAuCl_4{\cdot}4H_2O$ was 1:0.66, whereas the lower or higher mass ratio yielded decreased PEC response (S3, Figure S1). Therefore, a mass ratio of 1:0.66 was used in all of the other studies. The influence of reaction time and heating temperature on the AuNP diameter and PEC response was also examined. At 115 °C, 3 min, AuNPs were regular particles with size 26 ± 3 nm and uniform distribution and the PEC signal was the highest (S4, Figures S2 and S3).

To further explore the impact of the concentration variation of MB and *p*-NP toward self-powered PEC responses of AuNPs@ZnSeNS-modified GE, the concentration of MB and *p*-NP was changed. The MB is maintained at a certain concentration to investigate the variation of PEC response with the change of the concentration of *p*-NP. As shown in Figure 4, when 0.1 mM MB and 1 mM *p*-NP are used, PEC responses are much higher than other concentrations. The experimental results also show that when the concentration of MB is lower than 0.1 mM, the variation of *p*-NP concentration has little effect on the PEC signal and the PEC intensity is lower (Figure 4C,D). This fact suggested that in this MB and *p*-NP co-regulated self-powered PEC system, the concentration of MB is the main factor that governs the control functions. And the concentration of MB must maintain at a certain level. The higher or lower concentration of MB would give lower PEC signal (S5).

Mechanism of Co-Regulated Self-Powered PEC Response. To better study the PEC response mechanism, the CV of ZnSeNSs was measured (Figure 5A). As reported, the valence band (VB) edge energy level (E_{vb}), conduction band (CB) edge energy level (E_{cb}), and band gap (E_g) of semiconductor can be estimated from the onset positions of the oxidation and reduction waves in CV curves.[39,40] And the band positions of ZnSeNSs were obtained from the onset

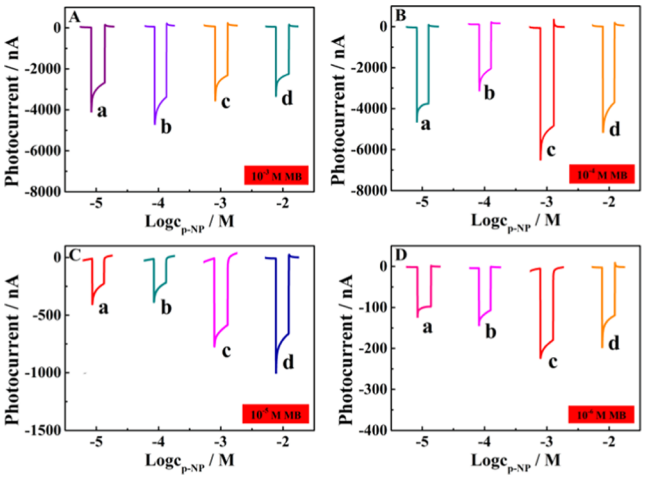

Figure 4. PEC response at different concentrations of MB and *p*-NP. The concentrations of MB are 1 mM (A), 0.1 mM (B), 0.01 mM (C), and 0.001 mM (D). The concentrations of *p*-NP are 0.01 mM (curve a), 0.1 mM (curve b), 1 mM (curve c), and 10 mM (curve d) in (A–D).

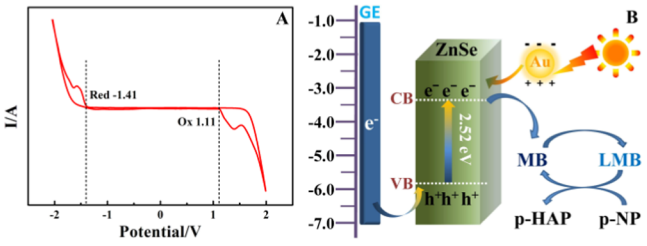

Figure 5. (A) CV of ZnSeNSs. (B) Mechanism of MB and *p*-NP co-regulated self-powered PEC response of AuNPs@ZnSeNSs.

oxidation potential (E_{ox}) and the onset reduction potential (E_{red}) using the following equations[41]

$$E_{VB/HOMO} = -(E_{ox} + 4.71)\text{eV} \quad (1)$$

$$E_{CB/LUMO} = -(E_{red} + 4.71)\text{eV} \quad (2)$$

$$E_{VB/HOMO} = E_{CB/LUMO} - \Delta E \quad (3)$$

According to the above equations, the VB and CB were found to be −5.82 and −3.30 eV, respectively, and the band gap (E_g) of ZnSeNSs was about 2.52 eV, which is slightly lower than the band gap of 2.67 eV for bulk ZnSe. As known, electron−hole pair generation is dependent on the band gap of ZnSeNSs. The decrease in band gap is useful for obtaining higher electron−hole pair generation, which improves the photocatalytic activity.[42] The PEC response mechanism of AuNPs@ZnSeNS-modified GE is shown in Figure 5B. When the energy of the visible light is greater than the energy required for the electron transition, the electron of VB was excited and then transited to CB forming electron−hole pairs under visible-light excitation. When AuNPs were loaded onto ZnSeNSs, the surface electrons on AuNPs, which were generated by SPR, were injected into the CB of ZnSeNSs, which restrain the recombination of photogenerated electron−hole pairs and thus enhance the photocurrent. Besides, the good conductivity of AuNPs also accelerates the electron transfer rate, further enhancing photocurrent. At the same time, the photogenerated electrons from the CB of ZnSeNSs rapidly transfer to MB, while the electrons from the gold

https://dx.doi.org/10.1021/acs.analchem.0c01893
Anal. Chem. XXXX, XXX, XXX−XXX

electrode transfer to the VB of ZnSeNSs to fill into photogenerated holes. Thus, the cathode photocurrent was produced. The presence of MB in solution plays two important roles: One is that MB as an electron acceptor can accept electrons from the CB of ZnSeNSs to decrease the recombination between electrons and holes to achieve amplification of PEC signals; the other is that after MB accepts electrons, it becomes LMB that can participate in redox reaction with *p*-NP, thereby realizing the reuse of MB and double amplification of PEC signals. The changes of UV−vis absorption spectra of MB and *p*-NP (S6, Figure S4) also confirmed these results.

Self-Powered PEC Strategy Coupling Recombinase Polymerase Amplification for Circulating Tumor Nucleic Acid Detection. Because the MB and *p*-NP co-regulated self-powered PEC strategy has eminent PEC response, it is used for nucleic acid detection with recombinase polymerase amplification (RPA). We developed a nucleic acid detection method with the MB and *p*-NP co-regulated self-powered PEC strategy coupled with in situ RPA on the surface of electrode. The prostate cancer circulating tumor nucleic acid biomarker, *KLK2*, is selected as target for the demonstration of proof of concept. Taking advantage of RPA amplification such as shorter amplification time (about 30 min), lower temperatures (25−42 °C) and less primers (2 primers), combining the co-regulated self-powered PEC strategy, we achieve attomolar circulating tumor nucleic acid detection.

As shown in Scheme 1, AuNPs@ZnSeNSs were first modified onto GE, and then SH-FP was immobilized onto

Scheme 1. Electron Acceptors Co-Regulated Self-Powered Photoelectrochemical Strategy and Its Application for Circulating Tumor Nucleic Acid Detection Coupled with Recombinase Polymerase Amplification[a]

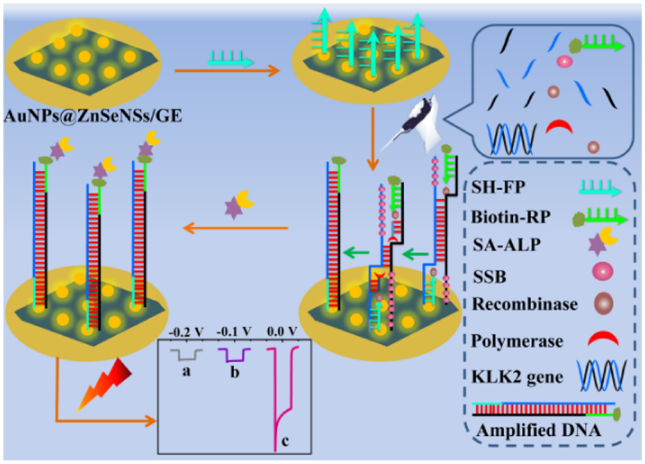

[a]Photocurrent of AuNPs@ZnSeNSs/GE in the presence of *p*-NP (a), MB (b), and MB and *p*-NP (c). SSB, single-strand DNA binding protein.

AuNPs@ZnSeNSs/GE by Au−S bonds. After adding a sample that contained *KLK2*, the SH-FP on the surface of electrode and biotin-RP in the solution result in RPA amplification in the presence of all enzymes and reagents contained in the TwistAmp Basic RT-RPA Kit necessary for transcription and amplification of *KLK2*. Then, the solid-phase RPA without thermocycling occurring on the electrode amplified the target and biotin-RP was captured at the surface of electrode. After washing, SA-ALP was attached through affinity between biotin and streptavidin. The ALP catalyzed the hydrolysis of *p*-NPP to *p*-NP. Benefiting from the high catalytic activity of ALP, many *p*-NPs were produced. Photoelectrochemistry is used to detect the photocurrent produced from MB and *p*-NP co-regulated self-powered PEC, and PEC signal is correlated to the *KLK2* gene level. The MB and *p*-NP co-regulated self-powered PEC strategy and RPA amplification allow for amplified signal detection with high sensitivity.

Characterization of MB and *p*-NP Co-Regulated Self-Powered PEC Assay. In the PEC *KLK2* assay, RPA is used for the target amplification. The feasibility of the target amplification is verified via polyacrylamide gel electrophoresis (PAGE)[43] (Figure 6A). The gel electrophoresis results

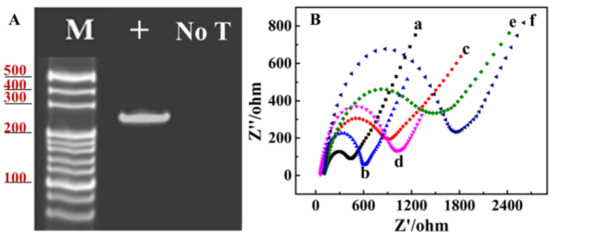

Figure 6. (A) PAGE analysis. +, positive sample; No T, no target. (B) EIS responses of the electrode stepwise modification process in 5.0 mM $[Fe(CN)_6]^{3-/4-}$ containing 0.1 M KCl: bare GE (a), AuNPs@ZnSeNSs/GE (b), SH-FP/AuNPs@ZnSeNSs/GE (c), MCH/SH-FP/AuNPs@ZnSeNSs/GE (d), after RPA on d (e), e incubated with SA-ALP (f).

indicated that the *KLK2* amplification process is successful. To further characterize the construction process of PEC assay step by step, EIS was performed in a 5.0 mM $[Fe(CN)_6]^{3-/4-}$ solution containing 0.1 M KCl. $[Fe(CN)_6]^{3-/4-}$ was used as a negatively charged redox label, and the semicircle diameter of impedance corresponded to the electron transfer resistance (Ret).[44] As shown in Figure 6B, the bare GE displayed a small Ret value (curve a). When AuNPs@ZnSeNSs was modified onto GE (curve b), the Ret value increased obviously, which was caused by the poor conductivity of ZnSeNSs. After SH-FP modified onto AuNPs@ZnSeNSs/GE (curve c), the Ret value was increased due to the lower conductivity of SH-FP. After the electrode was blocked by MCH, the Ret value further increased (curve d), which could be attributed to the electron transfer blocking of MCH. Finally, SH-FP, which was modified on AuNPs@ZnSeNSs/GE and biotin-RP in solutions, could recognize homologous nucleic acid sequence to get biotin-labeled DNA under the action of recombinase enzymes. Because phosphate groups of nucleic acid produced more negative charge onto the electrode surface and nucleic acid can increase steric hindrance, a significantly increased Ret was also observed (curve e). After RPA, SA-ALP was added. The Ret increased (curve f), which was attributed to the augment of steric hindrance. The EIS results from (curve a) to (curve f) suggested that the self-powered PEC assay had been successfully constructed.

Calibration Curve. As a proof-of-concept experiment, the detection of *KLK2* was investigated. Figure 7A presents PEC responses of different concentrations of *KLK2*. The PEC signals significantly increased when the concentrations of *KLK2* ranged from 5.0×10^{-17} M to 2.0×10^{-15} M (Figure 7B). A linear regression was plotted showing that the PEC signal was approximately proportional to the logarithm of

https://dx.doi.org/10.1021/acs.analchem.0c01893
Anal. Chem. XXXX, XXX, XXX−XXX

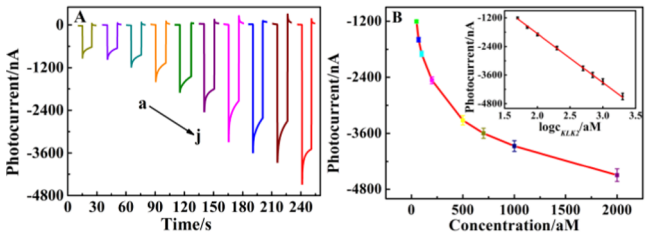

Figure 7. (A) PEC response of this PEC assay at different concentrations of *KLK2* from (a–j): 0, 30, 50, 70, 100, 200, 500, 700, 1000, 2000 aM. (B) The corresponding linear calibration plot for *KLK2* detection; the inset shows the log-linear correlation between PEC signal and the concentration of *KLK2* in the range of 50–2000 aM.

concentrations of *KLK2*. The regression equation was expressed as $I = -2027 \log c + 2185$ ($R^2 = 0.9992$) (c, *KLK2* concentration, aM). LOD was found to be 30 aM ($S/N = 3$, where S is the standard deviation and N is the slope) ($n = 11$). *PCA3* was also tested for application extension and verification. It exhibited a linear range of 40–1800 aM for *PCA3* detection with an LOD of 32 aM (Figure S5).

At the same time, to demonstrate good performance, a comparison of the reported self-powered PEC method with this work was explored. As shown in Table 1, the previously reported self-powered PEC assay achieved self-powered PEC performance by synthesizing new materials, while this work achieves self-powered PEC performance through the co-regulation of MB and *p*-NP. Moreover, this PEC assay had a wide detection range and a low detection limit (Table S1).

Specificity, Stability, and Reproducibility. To evaluate the specificity, the PEC responses of 5.0 fM *PCA3*, *SChLAP1*, *KLK3*, *TMPRSS2-ERG*, 500.0 aM *KLK2*, and their mixtures were detected, respectively. As shown in Figure 8A, only *KLK2* and mixtures showed high PEC responses. All of the others do not cause significant interference in the determination of *KLK2*, demonstrating the high specificity of this PEC assay for *KLK2* detection. This PEC assay also showed specificity for *PCA3* (Figure S6).

The stability of the MB and *p*-NP co-regulated self-powered PEC assay was measured under successive periodic "off–on–off" light for 12 cycles (Figure 8B). Under the continuous on/off cycle irradiation of 250 s, the PEC responses kept almost invariable. The stability of this PEC assay was due to the recycling of MB. The long-term stability was explored by measuring the MB and *p*-NP co-regulated self-powered PEC assay stored at 4 degrees every 5 days, and the PEC response shows no significant change in Figure 8C. Reproducibility of seven photoelectrodes PEC assays was also done. The RSD was 2.3% ($n = 7$) (Figure 8D). The results show that the MB and *p*-NP co-regulated self-powered PEC assay shows high stability and reproducibility.

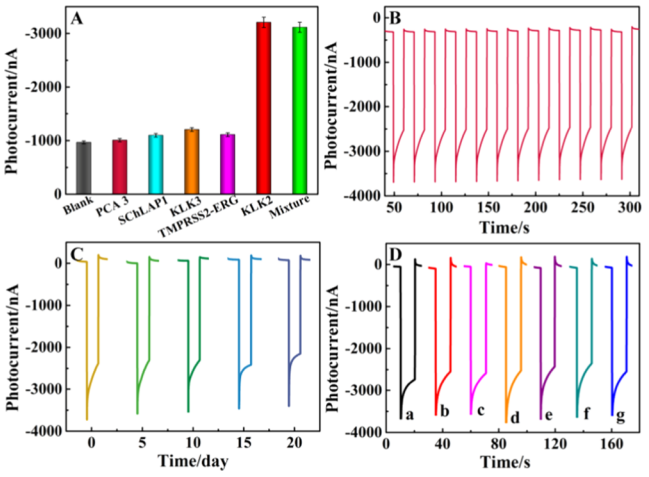

Figure 8. Specificity, stability, long-term stability, and reproducibility of MB and *p*-NP co-regulated self-powered PEC assay. (A) Specificity of this PEC assay with various interferents. (B) Stability of this assay under successive periodic "off–on–off" light for 12 cycles. (C) Long-term stability of this assay for 20-day storage. (D) Reproducibility of seven self-powered PEC assays (a–g). The concentrations of *KLK2* are all 1.0 fM for the stability and reproducibility measurements.

Sample Detection. To evaluate the applicability of this PEC assay for the detection of *KLK2* gene in real samples (S7), *KLK2* in serum samples of healthy people were detected by the standard addition method and the concentration of *KLK2* was also compared to that of quantitative real-time polymerase chain reaction (qRT-PCR). As shown in Table S2,

Table 1. Performance Comparison of This Self-Powered PEC Assay with Other PEC Assays for Bioactive Target Detection

mode[a]	photoactive material	target	linear range	LOD	refs
[b]	Co_3O_4-CNT-TiO_2[d]	glucose	0–4 mM	0.16 μM	16
[b]	Cu_2O/ZnO	GSH	10–1000 μM	0.42 μM	13
[b]	PbS QD/NiO	glucose	1 μM–10 mM	0.3 μM	45
[b]	IGZO/Si	glucose	0.055–55 mM		46
[b]	Au @ BiOI/NiO	glucose	0.1 μM–10 mM	0.0871 μM	14
[b]	Fe_2O_3NR	glucose	0.2–2.0 mM	5.5 μM	47
[b]	CdS/Eu-MOF	ampicillin	0.1–200 nM	0.093 nM	48
[b]	NiO/g-C_3N_4	oxytetracycline	0.01–100 nM	4 pM	20
[b]	CdSe/ZnS/TiO_2	gallic acid	1–200 μM	0.1 μM	8
[c]	AuNPs@ZnSeNSs	*KLK2*	50 aM–1 fM	30 aM	[e]

[a]According to self-powered PEC achieved by synthesizing photoactive materials with inherent self-powered features or regulated self-powered strategy, it can be divided into two categories. [b]Synthesizing new self-powered PEC materials. [c]Regulated self-powered strategy. [d]Co_3O_4-CNT-TiO_2: carbon nanotubes and Co_3O_4 deposits onto TiO_2; Cu_2O/ZnO: p-type Cu_2O film electrodeposits onto n-type ZnO nanorods array; PbS QD/NiO: PbS quantum-dot assembles onto the three-dimensional NiO nanostructured films; IGZO/Si: n-indium gallium zinc oxide/p-Si heterojunction; Au@BiOI/NiO: Au nanoparticles decorated three-dimensional bismuth oxyiodide nanoflower/two-dimensional nickel oxide nanosheet array; Fe_2O_3NR: hematite nanorod; CdS/Eu-MOF: CdS nanoparticles/europium metal–organic framework; NiO/g-C_3N_4: NiO nanocrystals/g-C_3N_4; CdSe/ZnS/TiO_2: CdSe/ZnS quantum-dot-sensitized TiO_2 nanoparticles; AuNPs@ZnSeNSs: Au nanoparticles@ZnSe nanosheets. GSH, glutathione. [e]This work.

https://dx.doi.org/10.1021/acs.analchem.0c01893
Anal. Chem. XXXX, XXX, XXX–XXX

when the *KLK2* gene was added to serum samples at different concentrations (0.1, 1.0, 5.0, 10.0 fM), it exhibited good recoveries from 96.7 to 103.8%, and the relative standard deviations (RSDs) are between 1.7 and 3.8%. The standard method qRT-PCR[49] shows that the results of this PEC assay are in good agreement with those obtained by qRT-PCR. The results demonstrate the feasibility and accuracy of this method for real sample analysis.

CONCLUSIONS

In summary, we reported a novel self-powered PEC sensing strategy. In this self-powered PEC sensing strategy, AuNPs@ZnSeNSs/GE gave the strongest PEC response with the co-regulation of MB and *p*-NP at 0 V. The direction of the photocurrent was also deflected at 0.1 and 0.2 V. Combining RPA amplification, a self-powered PEC assay was further fabricated for sensitive *KLK2* and *PCA3* detection with LODs of 30 and 32 aM, respectively. We envisioned that this concept of electron acceptors co-regulated self-powered PEC biosensing gave a new insight into the self-powered electrochemical and photoelectrochemical sensor and paved a new way to the development of new self-powered sensing platform without external electrical power supply.

ASSOCIATED CONTENT

Supporting Information

The Supporting Information is available free of charge at https://pubs.acs.org/doi/10.1021/acs.analchem.0c01893.

Experimental section, reagents, and apparatus (S1); preparation of ZnSe nanosheets (S2); effect of mass ratio of ZnSeNSs and $HAuCl_4 \cdot 4H_2O$ (S3, Figure S1); reaction time and heating temperature on PEC responses (S4, Figures S2 and S3); optimization of MB concentration (S5), UV−vis absorption spectra (S6, Figure S4); performance comparison for *KLK2* detection (Table S1); sample detection (S7, Table S2); and calibration plot and specificity for *PCA3* detection (Figures S5 and S6) (PDF)

AUTHOR INFORMATION

Corresponding Author

Xu Hun − *Key Laboratory of Optic-electric Sensing and Analytical Chemistry for Life Science, MOE; Shandong Key Laboratory of Biochemical Analysis; Key Laboratory of Analytical Chemistry for Life Science in Universities of Shandong; College of Chemistry and Molecular Engineering, Qingdao University of Science and Technology, Qingdao 266042, P. R. China;* orcid.org/0000-0001-5793-067X; Email: hunxuprof@outlook.com; Fax: +86 53284022681

Author

Yuchan Meng − *Key Laboratory of Optic-electric Sensing and Analytical Chemistry for Life Science, MOE; Shandong Key Laboratory of Biochemical Analysis; Key Laboratory of Analytical Chemistry for Life Science in Universities of Shandong; College of Chemistry and Molecular Engineering, Qingdao University of Science and Technology, Qingdao 266042, P. R. China*

Complete contact information is available at: https://pubs.acs.org/10.1021/acs.analchem.0c01893

Notes

The authors declare no competing financial interest.

ACKNOWLEDGMENTS

The authors thank the support of NSFC (21575073) and Laoshan Scholar Program of Qingdao Univ Sci & Technol (201802685).

REFERENCES

(1) Han, F.; Song, Z.; Nawaz, M. H.; Dai, M.; Han, D.; Han, L.; Fan, Y.; Xu, J.; Han, D.; Niu, L. *Anal. Chem.* **2019**, *91*, 10657−10662.
(2) Ge, L.; Liu, Q.; Hao, N.; Kun, W. *J. Mater. Chem. B* **2019**, *7*, 7283−7300.
(3) Jalali, M.; Moakhar, R. S.; Abdelfattah, T.; Filine, E.; Mahshid, S. S.; Mahshid, S. *ACS Appl. Mater. Interfaces* **2020**, *12*, 7411−7422.
(4) Zhang, L.; Luo, Z.; Su, L.; Tang, D. *Analyst* **2019**, *144*, 5717−5723.
(5) Najlaoui, D.; Echabaane, M.; Ben Khélifa, A.; Rouis, A.; Ben Ouada, H. *J. Solid State Electrochem.* **2019**, *23*, 3329−3341.
(6) Zhu, C.; Liu, D.; Li, Y.; Shen, X.; Li, L.; Liu, Y.; You, T. *Curr. Opin. Electrochem.* **2019**, *17*, 47−55.
(7) Çakıroğlu, B.; Demirci, Y. C.; Gökgöz, E.; Özacar, M. *Sens. Actuators, B* **2019**, *282*, 282−289.
(8) dos Santos, G. K. C.; da Silva, F. G. S.; Yotsumoto Neto, S.; dos Santos, W. T. P.; de Cássia Silva Luz, R.; Damos, F. S. *Electroanalysis* **2018**, *30*, 1750−1756.
(9) Li, C.; Han, C.; Zhang, Y.; Zang, Z.; Wang, M.; Tang, X.; Du, J. *Sol. Energy Mater. Sol. Cells* **2017**, *172*, 341−346.
(10) Zhao, K.; Yan, X.; Gu, Y.; Kang, Z.; Bai, Z.; Cao, S.; Liu, Y.; Zhang, X.; Zhang, Y. *Small* **2016**, *12*, 245−251.
(11) Zhang, C.; Chen, J.; Xuan, W.; Huang, S.; You, B.; Li, W.; Sun, L.; Jin, H.; Wang, X.; Dong, S.; Luo, J.; Flewitt, A. J.; Wang, Z. L. *Nat. Commun.* **2020**, *11*, No. 58.
(12) Grattieri, M.; Minteer, S. D. *ACS Sens.* **2018**, *3*, 44−53.
(13) Kang, Z.; Yan, X.; Wang, Y.; Bai, Z.; Liu, Y.; Zhang, Z.; Lin, P.; Zhang, X.; Yuan, H.; Zhang, X.; Zhang, Y. *Sci. Rep.* **2015**, *5*, No. 7882.
(14) Han, Q.; Wang, H.; Qi, Y.; Wu, D.; Wei, Q. *Nanoscale Adv.* **2019**, *1*, 4313−4320.
(15) Tian, J.; Zhu, H.; Chen, J.; Zheng, X.; Duan, H.; Pu, K.; Chen, P. *Small* **2017**, *13*, No. 1700798.
(16) Çakıroğlu, B.; Özacar, M. *Biosens. Bioelectron.* **2018**, *119*, 34−41.
(17) Gurudayal, G.; Beeman, J. W.; Bullock, J.; Wang, H.; Eichhorn, J.; Towle, C.; Javey, A.; Toma, F. M.; Mathews, N.; Ager, J. W. *Energy Environ. Sci.* **2019**, *12*, 1068−1077.
(18) Gai, P.; Kong, X.; Zhang, S.; Song, P.; Li, F. *Chem. Commun.* **2020**, DOI: 10.1039/D1030CC03039B.
(19) Yao, X.; Gao, J.; Yan, K.; Chen, Y.; Zhang, J. *Anal. Chem.* **2020**, *92*, 8026−8030.
(20) Duan, W.; Yan, P.; Dong, J.; Chen, Y.; He, X.; Chen, J.; Qian, J.; Xu, L.; Li, H. *Microchim. Acta* **2019**, *186*, No. 737.
(21) Shang, M.; Zhang, J.; Qi, H.; Gao, Y.; Yan, J.; Song, W. *Biosens. Bioelectron.* **2019**, *136*, 53−59.
(22) Yao, H.-B.; Mao, L.-B.; Yan, Y.-X.; Cong, H.-P.; Lei, X.; Yu, S.-H. *ACS Nano* **2012**, *6*, 8250−8260.
(23) Khater, M.; de la Escosura-Muñiz, A.; Altet, L.; Merkoçi, A. *Anal. Chem.* **2019**, *91*, 4790−4796.
(24) Gu, Y.; Sun, C.; Zhang, C.; Luo, X.; Xue, C.; Zhao, L. *CrystEngComm* **2019**, *21*, 5482−5491.
(25) Liu, H.; Jiang, Q.; Pang, J.; Jiang, Z.; Cao, J.; Ji, L.; Xia, X.; Wang, K. *Adv. Funct. Mater.* **2018**, *28*, No. 1703847.
(26) Belhout, S. A.; Baptista, F. R.; Devereux, S. J.; Parker, A. W.; Ward, A. D.; Quinn, S. J. *Nanoscale* **2019**, *11*, 19884−19894.
(27) Katz, E.; Bückmann, A. F.; Willner, I. *J. Am. Chem. Soc.* **2001**, *123*, 10752−10753.
(28) Zhou, L.; Liu, D.; Li, S.; Yin, X.; Zhang, C.; Li, X.; Zhang, C.; Zhang, W.; Cao, X.; Wang, J.; Wang, Z. L. *Nano Energy* **2019**, *64*, No. 103915.

(29) Wang, L.; Shao, H.; Lu, X.; Wang, W.; Zhang, J.-R.; Song, R.-B.; Zhu, J.-J. *Chem. Sci.* **2018**, *9*, 8482−8491.
(30) Zhang, Y.; Xu, W.; Xu, X.; Yang, W.; Li, S.; Chen, J.; Fang, X. *Nanoscale Horiz.* **2019**, *4*, 452−456.
(31) Cheng, Y.; Xu, Y.; Qian, Y.; Chen, X.; Ouyang, Y.; Yuan, W.-E. *Nano Energy* **2020**, *69*, No. 104411.
(32) Guo, H.; Pu, X.; Chen, J.; Meng, Y.; Yeh, M.-H.; Liu, G.; Tang, Q.; Chen, B.; Liu, D.; Qi, S.; Wu, C.; Hu, C.; Wang, J.; Wang, Z. L. *Sci. Rob.* **2018**, *3*, No. eaat2516.
(33) Kang, Z.; Gu, Y.; Yan, X.; Bai, Z.; Liu, Y.; Liu, S.; Zhang, X.; Zhang, Z.; Zhang, X.; Zhang, Y. *Biosens. Bioelectron.* **2015**, *64*, 499−504.
(34) Kang, Z.; Yan, X.; Wang, Y.; Zhao, Y.; Bai, Z.; Liu, Y.; Zhao, K.; Cao, S.; Zhang, Y. *Nano Res.* **2016**, *9*, 344−352.
(35) Yan, K.; Yang, Y.; Okoth, O. K.; Cheng, L.; Zhang, J. *Anal. Chem.* **2016**, *88*, 6140−6144.
(36) Kelley, S. O.; Barton, J. K.; Jackson, N. M.; Hill, M. G. *Bioconjugate Chem.* **1997**, *8*, 31−37.
(37) Wang, K.; Wu, C.; Wang, F.; Jiang, G. *ACS Appl. Nano Mater.* **2018**, *1*, 5843−5853.
(38) Zhang, J.; Cui, S.; Ding, Y.; Yang, X.; Guo, K.; Zhao, J.-T. *Biosens. Bioelectron.* **2018**, *112*, 177−185.
(39) Ručman, S.; Intra, P.; Kantarak, E.; Sroila, W.; Kumpika, T.; Jakmunee, J.; Punyodom, W.; Arsić, B.; Singjai, P. *Sci. Rep.* **2020**, *10*, No. 1388.
(40) Xing, G.; Liu, X.; Hao, S.; Li, X.; Fan, L.; Li, Y. *Nanomaterials* **2019**, *9*, 220.
(41) Barman, M. K.; Mitra, P.; Bera, R.; Das, S.; Pramanik, A.; Parta, A. *Nanoscale* **2017**, *9*, 6791−6799.
(42) Li, Z.; Zhang, S.; Xu, R.; Zhang, Q.; Wang, Z.; Fu, C. *Appl. Organomet. Chem.* **2019**, *33*, No. e5105.
(43) Koo, K. M.; Dey, S.; Trau, M. *ACS Sens.* **2018**, *3*, 2597−2603.
(44) Cheng, H.; Liu, J.; Ma, W.; Duan, S.; Huang, J.; He, X.; Wang, K. *Anal. Chem.* **2018**, *90*, 12544−12552.
(45) Dai, W.-X.; Zhang, L.; Zhao, W.-W.; Yu, X.-D.; Xu, J.-J.; Chen, H.-Y. *Anal. Chem.* **2017**, *89*, 8070−8078.
(46) Kim, K.; Kim, H.; Jang, H.; Park, J.; Jung, G.-Y.; Kim, M.-G. *ACS Appl. Mater. Interfaces* **2018**, *10*, 39487−39493.
(47) He, L.; Zhang, Q.; Gong, C.; Liu, H.; Hu, F.; Zhong, F.; Wang, G.; Su, H.; Wen, S.; Xiang, S.; Zhang, B. *Sens. Actuators, B* **2020**, *310*, No. 127842.
(48) Gao, J.; Chen, Y.; Ji, W.; Gao, Z.; Zhang, J. *Analyst* **2019**, *144*, 6617−6624.
(49) Hu, J.; Liu, M.-h.; Zhang, C.-y. *Chem. Sci.* **2018**, *9*, 4258−4267.

https://dx.doi.org/10.1021/acs.analchem.0c01893
Anal. Chem. XXXX, XXX, XXX−XXX